

Heat Transfer Characteristics for Practical Hydrogen Pressure Vessels Being Filled at High Pressure*

Peter L. WOODFIELD **, Masanori MONDE *** and Toshio TAKANO****

** National Institute of Advanced Industrial Science and Technology

744 Motoooka, Nishi-ku, Fukuoka 819-0395, Japan

*** Institute of Ocean Energy, Saga University

1 Honjo-machi, Saga, 840-8502, Japan

E-mail: monde@me.saga-u.ac.jp

**** JFE Container Company

9-2 Ukisima, Kawasaki-ku, Kawasaki, 210-0862, Japan

Abstract

Experiments have been conducted to measure the rise in temperature of hydrogen and vessel wall during filling of commercially available, practical tanks to 35 and 70 MPa. Three test vessels with volumes 205, 130 and 39 liters are investigated. The filling time ranges from 5 to 20 minutes. The heat transfer process is modeled using a one-dimensional unsteady heat conduction equation for the wall coupled with a flow and heat balance for the compressed gas. The model requires heat transfer coefficients between the hydrogen and the wall and the wall and surrounding air. Values of 500 W/(m²K) during filling, 250 W/(m²K) after filling for the inside wall and 4.5 W/(m²K) for the outside tank wall are tentatively assumed based on results from a previous study on a smaller vessel. The measured temperatures for the hydrogen gas and the wall are in good agreement with the calculations.

Key words: Hydrogen, Hydrogen Storage, CFRP, Pressure Vessel, Filling Hydrogen

1. Introduction

High pressure gas is presently the most widely used fuel storage mode for hydrogen vehicles. Typically fiber reinforced plastic (FRP) composite materials are used in order to reduce the weight of the vessel. While FRP has many desirable properties in relation to strength and weight, it is necessary to keep the material temperature below 85°C to maintain stringent safety requirements. Since this temperature can be exceeded through the compression work in the filling process, it is highly desirable to be able to predict the temperature rise. In the present study, experiments are performed on commercial FRP hydrogen storage vessels designed for mobile applications. Temperatures and pressures are measured during charging of three different vessels to 35 MPa or 70 MPa. Temperature characteristics are also measured for the hydrogen supply vessels.

Previously, the authors developed a thermodynamic model ⁽¹⁾ which couples an energy balance for the gas side with unsteady one-dimensional heat conduction for the wall. The gas is assumed to be perfectly stirred at all times. The same model is used in the present study but comparison is made with measurements from actual size vessels. Moreover, the model is modified to make it applicable to the supply vessels also. Details of the model are given in the appendix. The main results from the present study, recently presented in a slightly condensed form at a JSME-ASME conference ⁽²⁾, are now expanded and contain

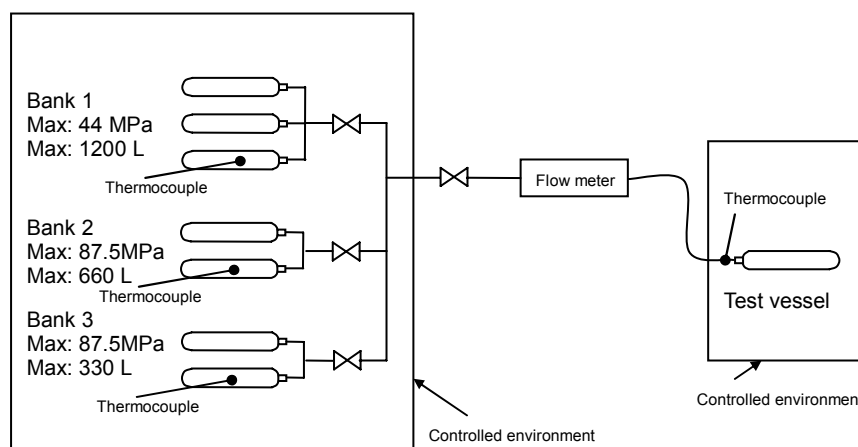


Fig. 1 Pressure vessel filling system (Powertech)

additional discussion concerning the effect of heat transfer in the piping system.

Nomenclature

a_s	: thermal diffusivity of solid
A	: inside surface area of pressure vessel
c	: specific heat for solid
C_p	: constant pressure specific heat for gas
h_a	: specific internal enthalpy of the supply
l	: total thickness of wall
m	: accumulated mass of H_2 in vessel
\dot{M}	: mass flow rate into vessel
P	: gas pressure
t	: Time
T_g	: gas temperature
T_s	: solid temperature
T_w	: wall inside surface temperature
u	: specific internal energy

Greek

α_h	: convection heat transfer coefficient from gas to wall
α_c	: convection heat transfer coefficient from wall to outside
λ	: thermal conductivity
ρ	: Density

2. Filling System Configuration and Test Vessel Geometry

The experiments were conducted at Powertech in Vancouver, Canada. The configuration of the hydrogen filling system used in the present study is shown in Fig. 1. The supply system is divided into three banks having vessels initially at 44 MPa and 87.5 MPa. This configuration is suitable for charging test vessels to 70 MPa. For 35 MPa runs only bank 1 was required. As shown in Fig. 1, gas temperatures are measured inside representative vessels in the supply banks and at the inlet to the test tank during filling. Tables 1 and 2 give the required properties of the material and geometry for the test vessels. Unfortunately, FRP samples from exactly the same vessels used in the present study were not available to measure the property data. The data shown in Table 2 is that of similar FRP material. The listed properties were measured at Saga University using the technique of Monde and

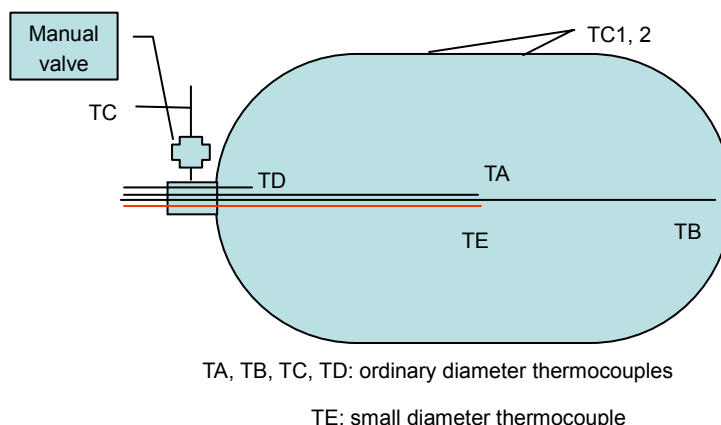


Fig. 2 Thermocouple positioning in test vessel

Mitsutake⁽³⁾. Table 3 gives the geometry of the storage banks.

Figure 2 shows the positioning of the thermocouples in the test vessel. The gas temperature inside the vessel is measured using four thermocouples and the outside wall temperature using two thermocouples. Thermocouples TA and TE have different hot-junction diameters and are located at approximately the same position to check the effect of the response time of the sensor. For the filling rates investigated in the present study thermocouples TA and TE gave very similar readings indicating that the ordinary diameter thermocouples were small enough. Pressures and temperatures of the filling system, surrounding environment and test vessel are monitored simultaneously during each test run.

Table 1: Specifications for test vessels

Vessel	A	B	C
Pressure / MPa	35	35	70
Volume / m ³	0.205	0.039	0.13
Area / m ²	2.33	0.685	1.32
FRP thickness / mm	17	11	43.5
Liner thickness / mm	4.25	3.25	5.25

Table 2: Wall property specifications

Material	Conductivity/(Wm ⁻¹ K ⁻¹)	Diffusivity/(m ² s ⁻¹)	Density/(kgm ⁻³)
FRP	0.55	0.45×10 ⁻⁶	1530
Al alloy	180	74.4×10 ⁻⁶	2700

Table 3: Geometry of storage banks

	Bank 1	Bank 2	Bank 3
Cylinder type	D	E	E
Max. No. of cylinders	8	4	2
Volume for single cylinder / m ³	0.15	0.165	0.165
Inside area for single cylinder / m ²	1.75	1.98	1.98
FRP thickness / mm	15.5	34	34
Al alloy liner thickness / mm	4.25	4.25	4.25
Heat transfer coefficient / Wm ⁻² K ⁻¹	250	250	250
External heat transfer coef. / Wm ⁻² K ⁻¹	4.5	4.5	4.5

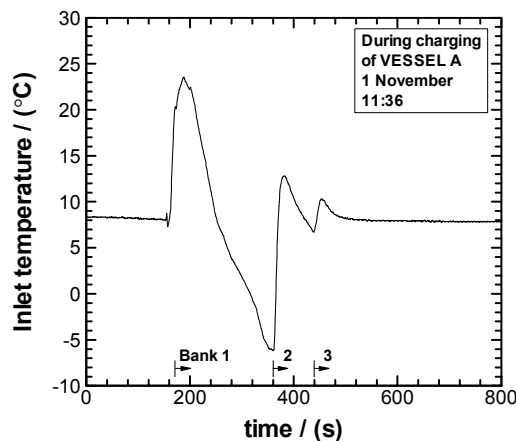


Fig. 3 Measured inlet temperature to test vessel during 5 minute fill

Concerning the 'Max. No. of cylinders' listed in Table 3 it is important to note that not all cylinders in each bank were used for every test. For any particular run the number of supply cylinders used can be found by considering the mass supplied to the test vessel and the corresponding pressure drop in the supply bank.

3. Measurement Results for Test Vessels

3.1 Test vessel inlet temperature

Figure 3 shows measured inlet temperatures to the 205L test vessel VESSEL A during filling to 35 MPa. Clearly the temperature is far from constant and is influenced strongly by the finite size of the supply vessels and pressure difference between the supply and test vessels. Hydrogen is supplied first from Bank 1 at time 170 s, then Bank 2 and finally Bank 3. For the example shown in Fig. 3, initially the inlet temperature rises steeply to a peak of around 24 °C. The temperature rise may be attributed to the negative Joule-Thomson coefficient for hydrogen as the gas passes through the regulator and partly to compression work on the gas in the supply line. The temperature change is not instantaneous at the start of the experiment due to the thermal inertia of the piping system. By about time 200 s (30 s after filling commenced) the temperature starts to fall and by time $t = 360$ s, a minimum of -6 °C is reached. Note that this is much lower than the ambient temperature of about 8 °C. The falling temperature after $t = 200$ s may be attributed almost entirely to the finite size of the supply bank. The gas inside the supply vessel does work pushing the gas out and thus the temperature in the vessel falls in a manner approximating adiabatic expansion. When the cold gas from the supply vessel passes through the regulator, isenthalpic expansion causes the temperature to rise again but the final temperature reaching the inlet to the test vessel is still quite low as shown in Fig. 3 for $300 < t < 360$ s. The same pattern is repeated for Banks 2 and 3.

3.2 Effect of inlet temperature on gas temperature in test vessel

Figure 4 shows the measured gas temperatures in the test vessel VESSEL A for a five minute filling time. Experimental data is given by symbols and lines show calculated results. In particular, the continuous dark line shows the calculated gas temperature using the present model. Two vertical arrows in Fig.4(b) give the times at which the supply tank is changed from one bank to another bank. These points correspond to the changes in trend from a falling temperature to a rising temperature in Fig.3.

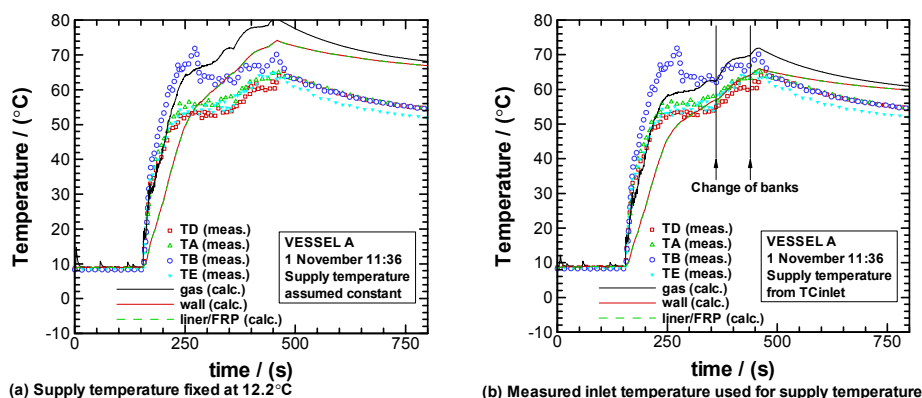


Fig. 4 Effect of test vessel inlet temperature on model predictions

In Fig. 4(a) the calculation is based on the assumption of an infinite supply vessel at a constant temperature of 12.2 °C (the initial temperature in the supply vessel for the test). On the other hand, Fig. 4(b) shows calculations where the inlet temperature was the measured supply temperature given in Fig. 3. To be consistent, the inlet pressure used for the calculation shown in Fig. 4(b) was taken to be the pressure of the test vessel rather than the pressure in the supply bank. This is appropriate because the drop in pressure across the regulator influences the inlet gas temperature via the Joule-Thomson effect. Clearly the inlet gas temperature has a significant effect on the model predictions and using the actual measured inlet temperature as the model input data yielded a better agreement between calculation and experiment.

There are two reasons why the calculated temperatures shown in Fig. 4(a) are in poorer agreement with experiment than in Fig. 4(b). Firstly, the actual supply temperature is not a constant value. This was shown in Fig. 3. However, secondly and more importantly, the main cause for the higher temperature predictions after about 300 s in Fig. 4(a) is the fact that the total enthalpy supplied to the vessel in the simulation for Fig. 4(a) is higher than in the experiment. In other words, the initial supply bank temperature of 12.2°C is too high to be used as an effective average inlet temperature. Reducing the model inlet temperature so that the average inlet enthalpy over the entire filling time is correct yields predictions for the gas temperature similar to those shown in Fig. 4(b). This is important to note since using a constant value may still be useful for predictions where the time history of the inlet temperature is not accurately known.

3.3 Performance of model for different filling times and different vessels

Figures 5 and 6 show results for different filling times and different vessels. Rather than using the measured inlet temperature changing with time, an effective constant inlet temperature was used so that the average inlet enthalpy matched the measured inlet condition. Figure 5 is for vessels that are filled to 35 MPa and on the whole, the agreement between model predictions and experiment is quite good.

The general tendency is for the model to over-predict the gas temperature. Note also that in Figs. 5(b), (d) and Fig. 6 the outside surface temperature of the pressure vessel was measured at two positions of TC1 and 2 and comparison with model predictions also quite good in many cases. The poorest agreement between model and experiment for the gas temperature is in Fig. 6 which shows results for a 130 L vessel charged to 70 MPa. In contrast to Fig. 5, the gas temperatures in Fig. 6 are around 20 °C higher than the measured temperatures when the vessel was full.

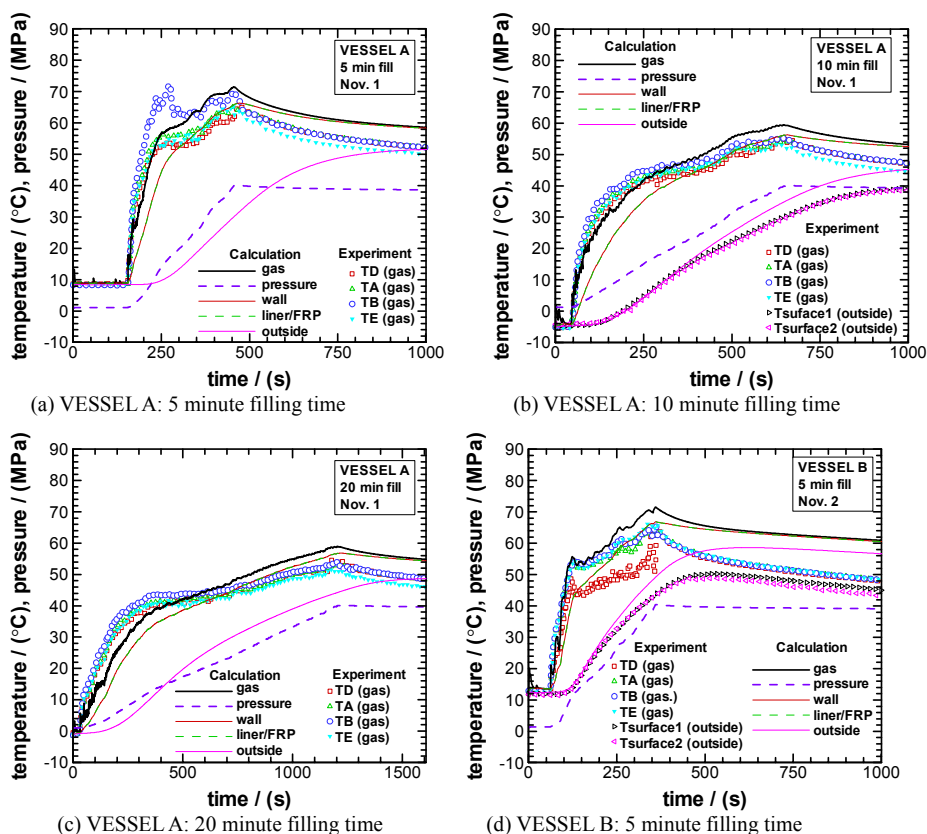


Fig. 5 VESSELS A and B with different filling times

3.4 Gas temperature distribution in the vessels

The thermodynamic model in this study assumes the gas is perfectly stirred and thus the model predictions are best interpreted as the space-averaged gas temperature. Considering the measured gas temperatures at different positions, it is clear that there is a consistent trend in the gas temperature distribution within the vessel. In many cases (e.g. see Figs 4 and 5), thermocouple TB, which is furthest from the inlet, shows the highest temperature reading. Conversely, thermocouple TD, which is closest to the inlet shows the lowest temperature. Three factors may contribute to this trend. Firstly, as may be expected from Fig. 3, since the inlet temperature is quite low, the temperature closer to the inlet may be influenced by this cooler gas. Secondly, the flow velocity gradually decreases with an increase in pressure and hardly reaches the furthest area. Thirdly, the gas flow further from the inlet may be less turbulent resulting in a poorer heat transfer coupling between the wall and the gas. Thus enhanced heat transfer near the inlet may be a factor contributing to reduction of the gas temperature for thermocouple TD. The small differences in temperature readings between thermocouples TA and TE may be attributed to the slightly different positions and to the difference in size of the hot-junction diameter.

3.5 The influence of the heat transfer coefficient during filling

In all cases shown in Figs. 4 to 6 it was assumed that the heat transfer coefficient was a constant value of $500 \text{ W}/(\text{m}^2\text{K})$ during filling. After filling the value was assumed to be $250 \text{ W}/(\text{m}^2\text{K})$ and $4.5 \text{ W}/(\text{m}^2\text{K})$ for the outside wall. These values were appropriate averaged values recommended by Monde et al.⁽¹⁾. In reality, however, one would expect that if filling is slower convection heat transfer would diminish. Thus for example, the heat transfer coefficient for Fig. 5(c) should be smaller than that for Fig. 5(a) or 5(b). This may explain

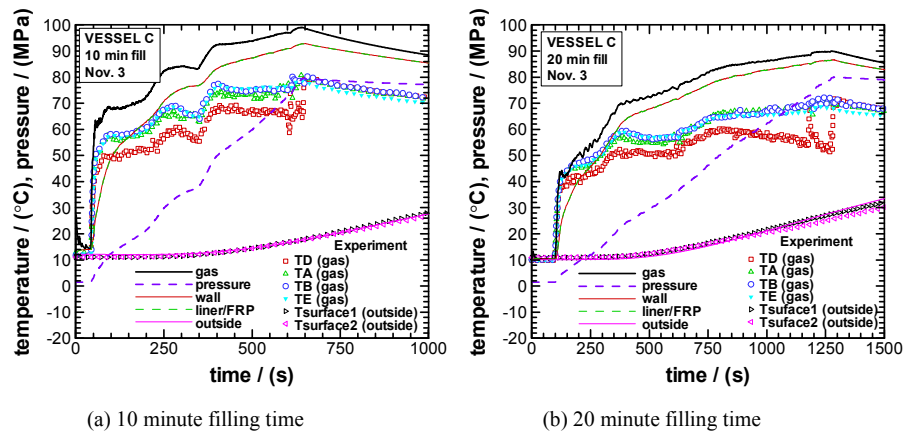


Fig. 6 VESSEL C with different filling times

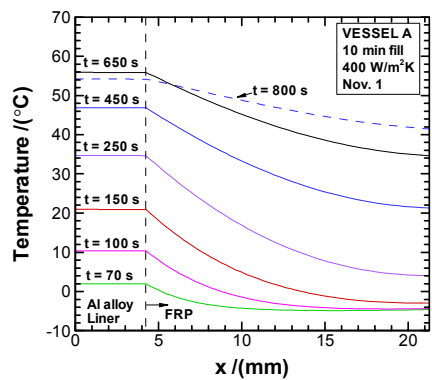


Fig. 7 Calculated temperature distribution in the wall

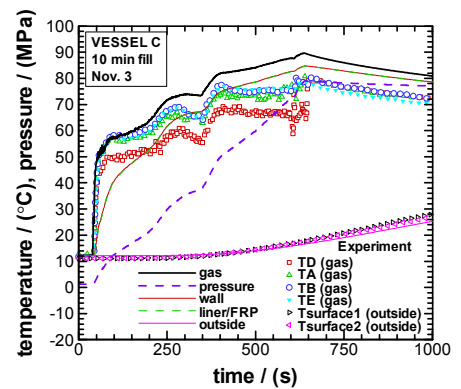


Fig. 8 Model liner thickness adjusted to correct liner mass (for case shown in fig. 6(a))

why during the first 400 seconds in Fig. 5(c), the model predictions are around 5 °C lower than measured gas temperatures. In fact, for example, by reducing the heat transfer coefficient to 400 W/(m²K) (not shown), much better agreement between the model and experiment during the first 200 seconds for the case in Fig. 5(b) can be achieved. It is worth mentioning that recently Woodfield et al.⁽⁶⁾ measured heat transfer coefficient during charging and discharging gas into a vessel and proposed a correlation to predict heat transfer. When charging hydrogen in the actual vessel at the corresponding velocity, the correlation gives the heat transfer coefficient to vary from about 500 to 300 W/(m²K) with decreasing its inlet velocity.

It is worth noting finally that the outside heat transfer coefficient has no effect on the gas temperature during the first few minutes since time is required for the thermal change to penetrate to outside wall. This is demonstrated in Fig. 7, which shows the calculated temperature distribution in the wall of the vessel at various times for the case considered in Fig. 5(b). In Fig. 7 the outside wall temperature ($x = 21.25$ mm) does not rise much from the initial value until time $t = 150$ s.

Another interesting observation from Fig. 7 is that the temperature in the aluminum alloy liner is almost uniform, in contrast to the FRP temperature distribution, which is non-linear. This implies that a simple lumped-capacity model for the FRP wall may be inappropriate. Note also that after the vessel was full ($t = 650$ s) the temperature of the liner starts to fall and the temperature distribution in the FRP starts to even out. This is shown by the dashed line marked $t = 800$ s.

3.6 The influence of thermal capacity of the wall

In general it may be concluded that the gas temperature is strongly influenced by the capacity of the wall to store and transmit heat. One weakness of the present model is that it assumes a constant thickness of liner and FRP for the entire pressure vessel. In reality however, both the liner and the FRP are considerably thicker in the dome regions at either end of the cylinder. Since the model neglects this extra heat capacity, model predictions should be conservative (i.e. yield an over-prediction of the maximum gas temperature).

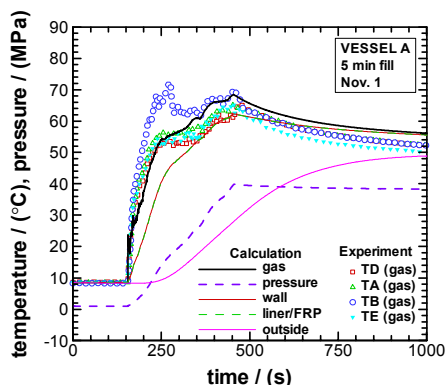


Fig. 9 Model liner thickness adjusted to correct liner mass (for case shown in Fig. 5(a))

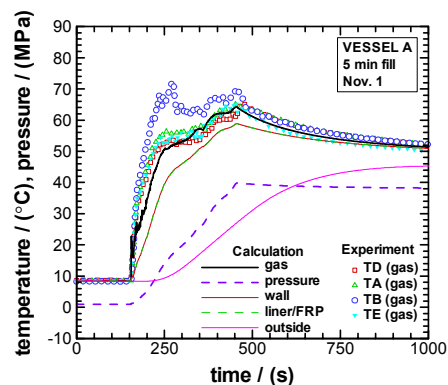


Fig. 10 Model liner inside surface area adjusted to correct liner mass (for case shown in Fig. 5(a))

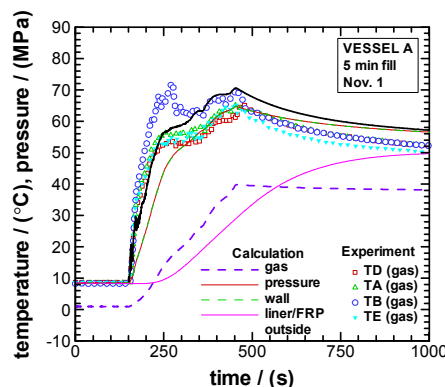


Fig. 11 Cylindrical coordinates used for heat conduction in the wall

This contributes to explaining the over-prediction of gas temperature for all of the cases shown in Figs. 5 and 6. In particular, the 70 MPa vessel, VESSEL C has a short aspect ratio and a very thick wall in the dome section in comparison to the cylindrical section of the vessel. To see if this extra heat capacity for the liner could explain the large over-prediction of temperature shown in Fig. 6, the calculation was repeated with the liner thickness adjusted so that the total mass of the liner was approximately correct. Figure 8 shows the result of this calculation. Comparing the gas temperature predictions in Figs 6(a) and 8 it is clear that the extra heat capacity in the dome section of the liner can explain most of the difference between the model results and experimental data.

For the cases shown in Fig. 5, even without any adjustment for the liner heat capacity, the agreement between calculation and experiment is quite good. In this case the cylindrical section of the vessel is large and correcting for the extra heat capacity in the dome does not have a major effect. Figure 9 shows the results for correcting the liner mass for the 205 L vessel. The change in gas temperature is not as dramatic as that for Fig. 8, but

comparing Figs. 9 and 5(a) it is clear that after the vessel is full ($t > 450$ s), the agreement between model and experiment is better for Fig. 9. This again confirms the importance of the total heat capacity of the liner.

3.7 The influence of the inner wall area

Heat transfer from the gas to the wall is also influenced by the inner wall area. The calculation was repeated with the same wall thickness as given in Table 1 but the wall area increased so that the heat capacity was close to the actual one including the extra mass in the dome. In principle this should lead to an underestimate of the gas temperature. Figure 10 shows the result of this calculation. Comparing the gas temperature in Figs. 9 and 10, one notices that the estimated temperature was improved to be closer to the measured one.

3.8 The influence of the wall curvature

Another point worth noting is that the present model assumes rectangular coordinates for heat conduction in the wall (see appendix). However, the effect of using cylindrical coordinates for the wall is not so great for the vessels considered in the present study. Figure 11 shows the same case shown in Fig. 5(a) recalculated with cylindrical coordinates for the wall. Comparing Figs. 11 and 5(a) it is clear that the effect of the chosen coordinate system for the wall is small.

4. Prediction of Temperature in Supply Banks

With a small modification as explained in the appendix, the same model used for filling may be used to predict the temperature during discharge of the supply vessel. The basic difference is that the enthalpy of the gas leaving the vessel is calculated based on the instantaneous temperature and pressure in the vessel itself rather than using a constant value

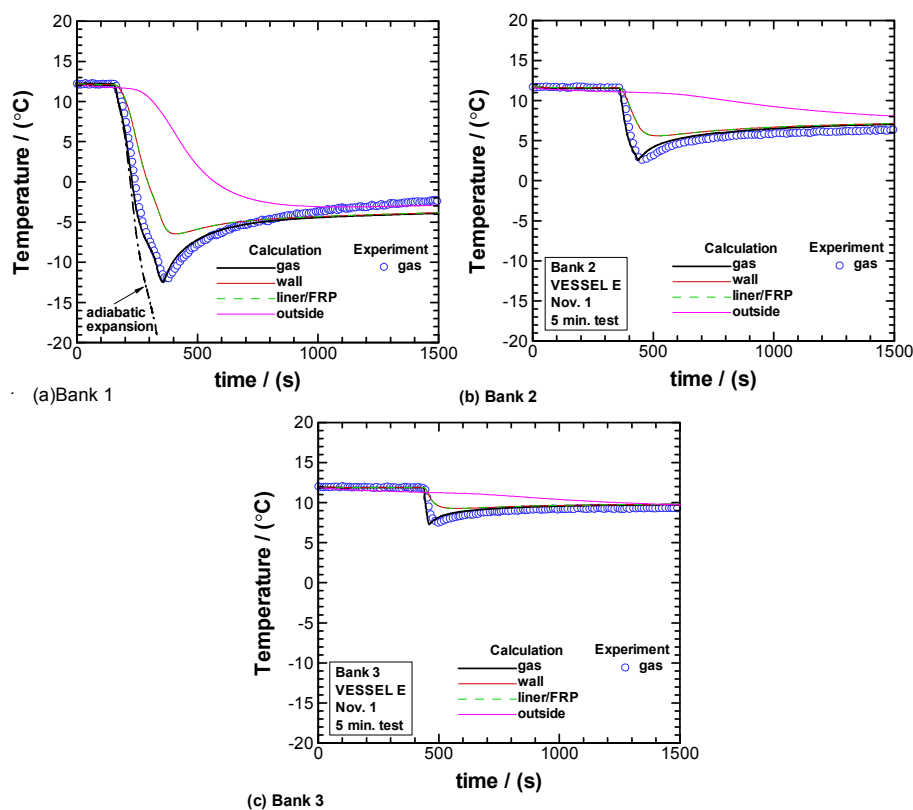


Fig. 12 Measurement and prediction of temperatures in supply vessels

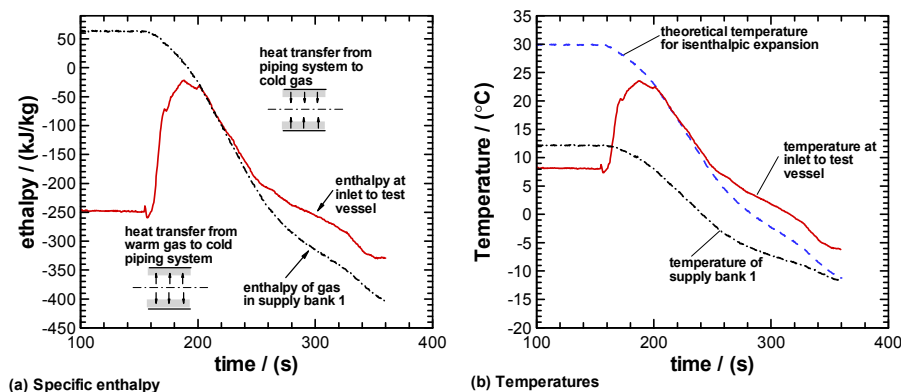


Fig. 13 Effect of heat transfer in the piping system between supply and test vessel

from the supply temperature and pressure. Figure 12 shows predictions and experimental data for the 5 minute filling case discussed previously in connection with Figs. 3 and 4. Note that experimental data was only collected for the gas temperature at a single point in one vessel from each bank. The dot-dash line in Fig. 12(a) is the estimated gas temperature change based on adiabatic expansion, namely no heat loss. The heat transfer coefficient during discharging was assumed to be a constant value of $250 \text{ W}/(\text{m}^2\text{K})$ for all of the supply banks. Using this value, comparison between the measured gas temperature (symbols) and calculated gas temperature (dark line) is excellent. It is worth mentioning that in a short time after discharging, the measured temperature agrees with the dot-dash line so that it behaves as adiabatic expansion, and after that the temperature is gradually shifted upward by the influence of the heat transfer from the wall.

It is also interesting to compare Fig. 12 with Fig. 3, which shows the gas temperature at the inlet to the test vessel for the same run. Note that the temperature in Bank 1 (Fig. 12(a)) becomes much colder ($-12 \text{ }^\circ\text{C}$) than the minimum temperature at the inlet to the test vessel ($-6 \text{ }^\circ\text{C}$). The temperature rise between the supply vessel and the inlet to the test vessel is due to the negative Joule-Thomson coefficient for hydrogen as it passes through the regulator.

5. Enthalpy Difference between the Supply Bank and Test Vessel

The enthalpies at the exit of the supply tank and inlet of the test vessel can be calculated from the pressure and either the estimated or measured temperature. Figure 13(a) shows the enthalpy change with time during which hydrogen gas is supplied from the bank 1. Enthalpies are calculated relative to the reference point $25 \text{ }^\circ\text{C}$, 0.1013 MPa where the enthalpy is taken to be zero. Initially and even after filling starts, the specific enthalpy of the gas in the supply bank is higher than the specific enthalpy at the inlet to the vessel. The reason for this is that heat transfer occurs between the warm gas and the cold pipeline before the hydrogen enters the vessel. When the gas passes through the regulator the enthalpy should be almost constant resulting in a temperature rise due to the negative Joule-Thomson coefficient. Heat is then transferred from the warmer gas to the colder pipeline so that the enthalpy of the gas at the inlet to the vessel is lower. However as filling progresses, the temperature of the gas in the supply bank decreases due to the work done pushing the gas out of the vessel. The temperature of the supply bank is shown by the black dash-dot line in Fig. 13(b). At some point in time ($t \approx 220 \text{ s}$) the temperature in the supply bank is sufficiently low so that even with the increase in temperature due to the negative Joule-Thomson coefficient, the gas temperature downstream of the regulator becomes lower than the temperature of the piping system. After this, heat is transferred from the piping

system to the colder gas. This explains the observation in Fig. 13(a) that after about $t = 220$ s, the specific enthalpy of the hydrogen at the inlet to the test vessel is higher than the specific enthalpy of the hydrogen in the supply bank.

Figure 13(b) compares the measured temperature at the inlet, the measured temperature in the supply bank and the theoretical temperature for isenthalpic expansion. The temperature calculated from isenthalpic expansion is always greater than the temperature in the supply bank because of the negative Joule-Thomson coefficient. The difference between the blue dashed line and the red solid line in Fig. 13(b) shows the importance of heat transfer between the gas and the supply piping system.

6. Conclusions

The main conclusions from this fast-fill study conducted at Powertech in Canada are as follows.

1. The temperature of the hydrogen during charging of three different vessels was measured and compared well with predictions from the analytical model.
2. The model also successfully predicted the temperatures in the supply vessels during discharge.
3. Differences between predictions and experiment can be explained by the fact that the model neglects the extra thermal capacity of the liner and FRP in the dome sections of the cylinders.
4. Heat transfer in the pipeline has an important influence on the temperature of the gas entering the test vessel.

Acknowledgement

The authors would like to express appreciation to New Energy and Industrial Technology Development Organization (NEDO) for financial support to this research.

Appendix: Thermodynamic Model for Charging Hydrogen into Vessel and Discharging from Vessel

Figure A1 gives an overview of the present model. The supply enthalpy, h_a is calculated either using a fixed supply temperature and pressure (infinite source size) or as a function of time using the measured inlet temperature and pressure.

Assuming the gas temperature is uniform throughout the vessel, conservation of energy for the gas side is given by Eq. (A1).

$$\alpha_h A (T_w - T_g) + \dot{M} h_a = \frac{d}{dt} (m u(P, T_g)) \quad (A1)$$

α_h is the convection heat transfer coefficient to the wall, A is the inside surface area of the vessel, T_w is the wall inside surface temperature and T_g is the gas temperature. The density required to calculate the mass, m in the vessel is given by the real-gas equation of state specified in Eq. (A2). The compressibility, Z , is calculated using a polynomial fit to hydrogen gas data generated the Lee-Kesler method⁽⁴⁾. This data agreed well with tabulated compressibility data⁽⁵⁾ for hydrogen in the range of temperatures considered in this study.

$$\rho(P, T_g) = \frac{P}{Z(P, T_g) R T_g} \quad (A2)$$

It is worth noting that for discharge gas, the enthalpy for the discharged gas in Eq.(A1)

is identical to that in the vessel.

The wall is assumed to behave as a one-dimensional solid, thus conservation of energy for the wall may be described by unsteady heat conduction, Eq. (A3).

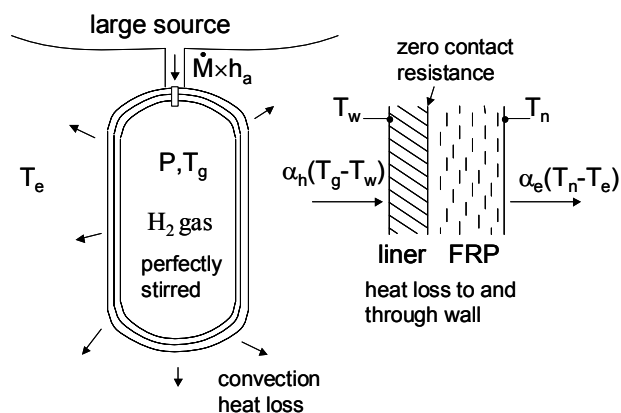


Fig. A1 Schematic diagram of thermodynamic model

$$\frac{\partial T_s}{\partial t} = a_s \frac{\partial^2 T_s}{\partial x^2} \quad (A3)$$

The boundary conditions for Eq. (A3) are given by Eqs. (A4) and (A5)

$$-\lambda_s \frac{\partial T_s}{\partial x} \Big|_{x=0} = \alpha_h (T_g - T_s \Big|_{x=0}) \quad (A4)$$

$$-\lambda_s \frac{\partial T_s}{\partial x} \Big|_{x=l} = \alpha_e (T_s \Big|_{x=l} - T_e) \quad (A5)$$

Here $T_w \equiv T_s|_{x=0}$ and l is the total thickness of the wall. The initial condition is taken to be a uniform temperature. It should be mentioned that the temperature and heat flux at the interface between liner and FRP have the identical values for them and the thermal properties are also used for the liner and FRP, respectively.

The system of equations is closed by specifying the measured pressure in the vessel as a function of time until the vessel is full. After filling, the mass in the vessel is assumed constant and the pressure is calculated as the vessel cools. The heat transfer coefficients, α_h and α_e for inside and outside surfaces of the vessel are assumed to have values of $\alpha_h=500$ W/(m²K) during filling, $\alpha_h=250$ W/(m²K) after full and $\alpha_e=4.5$ W/(m²K) for all conditions. During discharging α_h is assumed to be 250 W/(m²K), the sign of mass in Eq. (A1) becomes negative and the enthalpy leaving the vessel, h_a is calculated based on the instantaneous temperature and pressure in the vessel.

The above equations are solved simultaneously using the finite-volume method to discretize Eq. (A3) and a bisection search algorithm is used to couple this result with energy conservation for the gas side, Eq. (A1).

References

- (1) M. Monde, Y. Mitsutake, P. L. Woodfield, S. Maruyama, Characteristics of Heat Transfer and Temperature Rise of Hydrogen during Rapid Hydrogen Filling at High Pressure, *Heat Transfer – Asian Research*, Vol. 36 (2007) pp. 13-27.
- (2) P. L. Woodfield, T. Takano, M. Monde, Characteristics of Heat Transfer for Hydrogen and Wall During Filling Hydrogen into Actual Tank at High Pressure, HT2007-32550, *Proceedings of ASME-JSME Thermal Engineering Summer Heat Transfer Conference*, Vancouver, July 2007.

- (3) M. Monde, Y. Mitsutake, A new estimation method of thermal diffusivity using analytical inverse solution for one-dimensional heat conduction, *International Journal of Heat and Mass Transfer*, Vol. 44 (2001) pp. 3169-3177.
- (4) B. I. Lee, M. B. Kesler, A generalized thermodynamic correlation based on three-parameter corresponding states, *AIChE Journal*, Vol. 21 (1975) pp. 510-527.
- (5) R. H. Perry, D. W. Green, J. O. Maloney, Perry's Chemical Engineers' Handbook, 7th Edition, McGraw-Hill, USA, pp. 2-224 – 2-245, 1997.
- (6) P. L. Woodfield, M. Monde, Y. Mitsutake, Measurement of average heat transfer coefficients in high-pressure vessel during charging with hydrogen, nitrogen or argon gas, *J. of Thermal Science and Engineering*, Vol.2, No.2, (2007), pp.180-190.